Energy Engineering

Tech Science Press

Doi:10.32604/ee.2025.073663

ARTICLE

Inertia Support Coordinated Control Strategy for Wind Power Connected to the Grid through MMC-HVDC Considering Secondary Frequency Drop

Yi Qi[1], Yuhao Xie[2,*], Zhibing Hu[1], Fan Ding[1], Junxian Ma[3], Liang Zhao[3] and Shouqi Jiang[2]

[1]Economic and Technological Research Institute, State Grid Ningxia Electric Power Co., Ltd., Yinchuan, 750000, China
[2]School of Electrical Engineering, Northeast Electric Power University, Jilin City, 132012, China
[3]State Grid Ningxia Electric Power Co., Ltd., Yinchuan, 750000, China

*Corresponding Author: Yuhao Xie. Email: jsq@neepu.edu.cn

Received: 23 September 2025; Accepted: 20 November 2025; Published: 30 August 2026

ABSTRACT: To address the challenges of low inertia support capability and poor frequency stability encountered in the process of power system electronification, this paper designs a coordinated inertia support control strategy for offshore wind power connected to the grid via Modular Multilevel Converter Based High Voltage Direct Current (MMC-HVDC), which enhances the system inertia level and accounts for secondary frequency drop. In terms of inertia support, building on the existing coupling relationship between grid frequency and DC voltage, the influence of wind turbine (WT) rotor speed is further integrated, leading to the proposal of a virtual inertia control method that synergistically leverages the frequency regulation capabilities of sub-module (SM) capacitors and WTs. Meanwhile, to mitigate the power impact on the system at the instant WTs exit inertia support control, an adaptive rotor speed recovery strategy based on a variable droop coefficient designed using a logistic function is proposed, along with an adaptive submodule switching control method that utilizes the MMC-HVDC capacitor energy margin to compensate for the power deficit caused by wind turbine rotor speed recovery. Compared with existing wind power recovery methods, the coordinated operation of these two strategies can prevent secondary frequency dips while shortening the rotor speed recovery time. Finally, the simulation verification was carried out based on the RTLAB OP5707XG-8 real-time digital simulation platform, where the installed capacity of the wind farm is 600 MW, and the results show that the original system experiences a secondary frequency dip of approximately 0.0013 p.u., whereas no secondary frequency dip occurs when the proposed method is applied, and the recovery time is shortened by about 5 s, demonstrating the effectiveness of the proposed coordinated control strategy.

KEYWORDS: Offshore wind farms connected to the grid through MMC-HVDC transmission; inertia support; secondary frequency drop; speed recovery; power impact; coordinated control

1 Introduction

Offshore wind power is rich in resources, boasts long utilization hours, imposes minimal environmental impact, and holds enormous development potential [1,2]. Thanks to its high stability, strong support capability, and flexible control, the MMC-HVDC has become the key solution for integrating large-scale offshore wind power [3–5].

As the grid-connected capacity of offshore wind power using MMC-HVDC technology continues to rise [6–8], traditional frequency modulation resources are gradually being replaced, resulting in a decline in the overall inertia level of the system and exerting a serious impact on frequency stability [9–11]. For instance, the 14 August 2003 California blackout, the 9 August 2019 UK blackout, and the 19 September 2019 East China frequency drop event (maximum deviations reaching up to 0.2 Hz) all involved rapid frequency decline or generator tripping due to insufficient inertia. Against this backdrop, it is particularly important to achieve active inertia support from offshore wind power through the MMC-HVDC interconnected system [12]. Existing control methods mainly rely on communication links or DC voltage to transmit the frequency information of the receiving-end grid. By regulating the active power outputs of the MMC-HVDC system and the wind farm, these methods adjust the capacitor energy and rotor kinetic energy to actively participate in power imbalance regulation and enhance system frequency stability. Reference [13] proposes a Generator Emulation Control (GEC)-based method with reference to the inertia model of generators, thereby enabling converter stations to provide synthetic inertia. Reference [14] dynamically adjusts the number of MMC SMs based on the DC voltage difference, which effectively suppresses the rate and magnitude of frequency fluctuations. References [15,16] calculate the additional components of WT-related control variables based on the frequency deviation and the coupling relationship between DC voltage and WT rotor speed, respectively, thus achieving effective support for system inertia. For wind power grid-connected systems integrated into multi-terminal direct current (MTDC) grids, relevant studies have proposed various optimization schemes and control strategies. Reference [17] presents a novel frequency dynamic constrained unit commitment (FDUC) scheme, and Reference [18] designs an auxiliary dead-band controller (ADC) scheme, both of which effectively improve the power transmission capacity of the system. Reference [19] ensures the stable operation of the MTDC system when power imbalances occur in multiple Alternating Current (AC) grids by transferring the recovery power of WTs to undisturbed AC grids. The Reference [20] enhances the voltage variation range of the supercapacitor by connecting it to the DC bus of the WT system, thereby maximizing the utilization of the capacitor's energy storage capacity and improving the overall inertia level of the system.

The frequency response process of offshore wind power mainly includes two stages: inertia support and speed recovery. The control strategy switching at the end of the inertia support stage will lead to an instantaneous drop in its output power, thereby causing the problem of secondary frequency drop and further threatening the stability of the system [21]. Research on methods to suppress secondary frequency drops mainly focuses on optimizing WT frequency response parameters, adding energy storage devices, and adjusting the electromagnetic power increment of WTs. Reference [22] proposes a multi-objective adaptive inertia and droop control method for WTs that balances active power frequency support and rotor speed recovery, achieving effective suppression of secondary frequency drops. Reference [23] considers the economic efficiency of energy storage and divides the wind-storage combined frequency regulation into three distinct stages based on the frequency response capability of WTs. It configures the energy storage response power according to the control objectives of each stage, thereby avoiding the occurrence of secondary frequency drops. For offshore wind farms connected to the power grid via MMC-HVDC, based on the coupling relationship between the frequency of the receiving-end power grid and the DC voltage, Reference [24] multiplies the increment of the output electromagnetic power of the WT by a variable-rate recovery function, which takes both the speed recovery time and the suppression of secondary frequency drop into account. Reference [25] utilizes WTs adopting a load-shedding strategy to provide energy reserves, thereby compensating for the power deficit during the rotor speed recovery stage. It can be seen from this that existing References mainly focus on the relevant control methods of WTs, while there are relatively few studies on coordinated control that take into account the regulation capability of MMC-HVDC and the recovery speed of WT rotor speed. Therefore, fully tapping the supporting potential of the MMC-HVDC system and enabling it to assist in the rotor speed recovery of offshore wind power is of great significance for ensuring the safe and stable operation of the system frequency.

Under this background, this paper proposes an inertia support coordinated control strategy for wind power connected to the grid through MMC-HVDC considering secondary frequency drop. The principal contributions made by this paper are presented as follows:

(1) As for offshore wind power: the coupling relationship among grid frequency, DC voltage, and WT rotor speed is established, and a virtual inertia control (VIC) strategy and an adaptive rotor speed recovery strategy with a variable droop coefficient have been designed, which is proposed via a novel recovery function adhering to the "slow-then-fast' principle". Compared with conventional fixed-droop methods, they can effectively reduce the instantaneous power impact on the system caused by the withdrawal of inertia support control from the wind farm.

(2) As for MMC-HVDC: adaptive switching strategies and related control parameters for MMC SMs at the sending and receiving ends are designed, respectively, according to the WT rotor speed recovery state and DC current variation. While wind power and MMC jointly support the system inertia, the coordinated recovery of the two is simultaneously achieved, using the capacitor energy margin to adaptively support WT rotor speed recovery. Compared with conventional WT self-recovery methods, this approach effectively prevents secondary frequency dips, shortens turbine recovery time, and enhances overall system security and stability.

The rest of the paper is organized as follows: Section 2 introduces the system structure and its power support requirements. Section 3 designs the VIC strategies for MMC and WTs. Section 4 proposes the coordinated control strategy for secondary frequency drop mitigation. Section 5 presents case studies and simulation results. Section 6 draws conclusions.

2 Structure of Offshore Wind Farms Connected to the Grid through MMC-HVDC Transmission

Fig. 1 shows the structure of the offshore wind power grid-connected system via MMC-HVDC, which adopts a symmetric monopole topology as the main wiring configuration. Specifically, the sending-end MMC adopts constant frequency/AC voltage (f/U_{ac}) control to provide voltage and frequency support for offshore wind power; while the receiving-end MMC adopts constant DC voltage/constant reactive power (U_{dc}/Q) to ensure the reliability of power transmission. The key system parameters will be presented in the simulation verification section, as shown in Table 1.

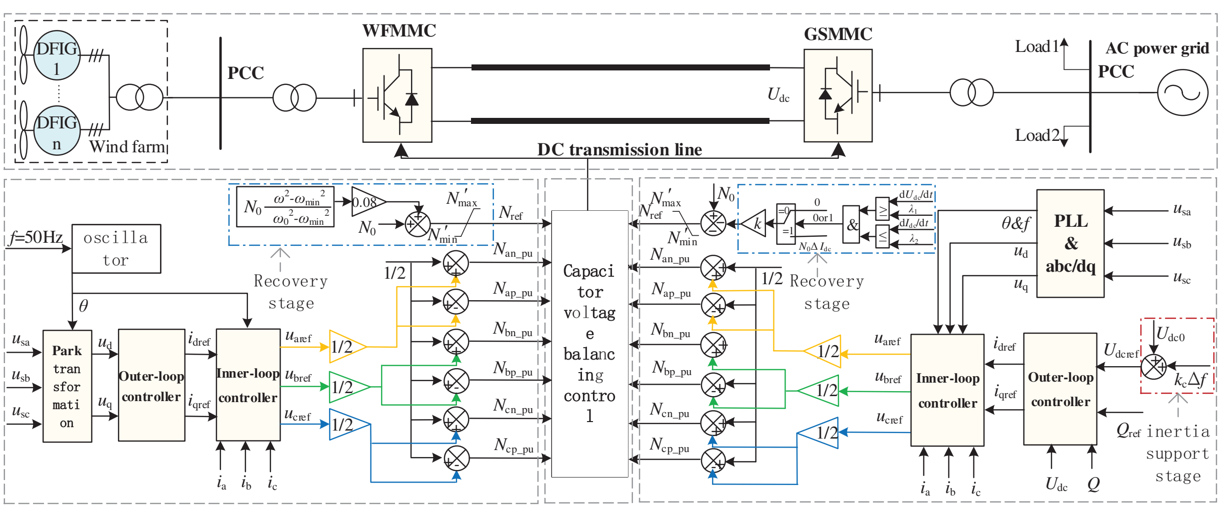

Figure 1: Structure of offshore wind farms connected to the grid through MMC-HVDC transmission

Table 1: Main parameters of the simulation system

Parameter	Sending-End MMC	Receiving-End MMC
Grid-side voltage	220 kV	500 kV
Valve-side voltage	260 kV	260 kV
Capacity	1500 MVA	1500 MVA
DC voltage	500 kV	500 kV
Number of bridge arm SMs	228	228
SM capacitance	15 mF	15 mF
Arm inductance	75 mH	75 mH
Coupling coefficient k_c	5	5
Proportional coefficient k	/	0.8

For the MMC-HVDC system, the system equivalent DC-side capacitance C_{eq}, the sending-end DC voltage U_{dc}, the sending-end forward active power P_{in}, and the active power P_{out} injected into the AC power grid by the receiving end have the following relationships:

$$C_{eq}U_{dc}\frac{dU_{dc}}{dt} = P_{in} - P_{out} \tag{1}$$

On the sending-end AC side, P_{in} can be expressed as:

$$P_{in} = \frac{1}{X_L}U_{WF}U_{ac}\sin\delta \tag{2}$$

where U_{WF} is the voltage of the WT grid-connection point, U_{ac} is the AC-side voltage of the sending-end MMC, X_L represents the equivalent reactance, and δ is the phase angle difference between U_{WF} and U_{ac}.

When a power disturbance occurs in the receiving-end power grid, which will result in a change in P_{out}, the DC voltage will vary accordingly as indicated by Eq. (1). However, under conventional constant DC voltage control, the MMC-HVDC system regulates its output power back to the initial value to maintain DC voltage stability, and therefore does not participate in system power imbalance regulation. In the absence of communication, the offshore wind farm cannot perceive the frequency variation of the receiving-end grid, and its injected DC power P_{in} remains unchanged, making it unable to provide frequency support to the receiving-end power system. With the increasing penetration of renewable energy, the frequency security and stability of the power system will face severe challenges. Therefore, based on the DC voltage reflecting the frequency variations of the receiving-end grid, and incorporate it into the active power control loop of the offshore wind farm, using the DC capacitor energy and wind turbine rotor kinetic energy to participate in suppressing the system frequency change rate and maximum frequency deviation, it is of great significance for maintaining frequency security and stability. Given the high probability and significant impact of load variations during system operation, this paper focuses on the frequency drop condition. On the basis of fully exploring the frequency regulation capabilities of the MMC-HVDC and wind farms, this paper proposes a coordinated control strategy that balances active inertia support and rapid rotor speed recovery of WTs, thereby ensuring the safe and stable operation of the system. The specific control method will be described in detail later in the paper.

3 Virtual Inertia Control Strategy

Inertia response refers to the process in which the internal energy storage elements of a power system release or absorb energy to adjust the active power injected into the AC grid when a disturbance occurs, typically taking place in the initial stage of the disturbance to provide short-term support. To effectively address the abrupt frequency changes caused by power imbalance, this paper designs a VIC strategy by leveraging the energy stored in MMC DC capacitors and WT rotors to mitigate the frequency change rate in the initial stage of disturbances.

3.1 Virtual Inertia Control Based on DC Capacitor Energy Storage

Building on Reference [14], system frequency deviation is introduced into the DC voltage control loop of the receiving-end MMC, and a correlation between DC voltage and grid frequency is established. This enables active participation in the system frequency regulation while providing conditions for the sending-end MMC and offshore wind power to support the system inertia.

$$U_{\mathrm{dcref}} = U_{\mathrm{dc0}} + \Delta U_{\mathrm{dc}} = U_{\mathrm{dc0}} + k_{\mathrm{c}} \Delta f \tag{3}$$

where U_{dcref} is the DC voltage reference value set by GSMMC; U_{dc0} and U_{dc} are the rated value and actual value of DC voltage, respectively; $\Delta U_{\mathrm{dc}} = U_{\mathrm{dc}} - U_{\mathrm{dc0}}$ is the DC voltage deviation; $\Delta f = f - f_0$ is the frequency variation; k_{c} is the coupling coefficient between DC voltage deviation and frequency deviation.

Since $\Delta f \propto \Delta U \propto U_{\mathrm{dcref}}$, and U_{dcref} may exceed the voltage stability range (±5%) as f decreases, the DC voltage can only transmit part of the frequency variation characteristics. To this end, the coupling coefficient k_{c} is set as follows:

$$k_{\mathrm{c}} = \frac{\Delta U_{\mathrm{dcmax}}}{\Delta f_{\mathrm{max}}} \tag{4}$$

where $\Delta U_{\mathrm{dcmax}}$ and Δf_{max} are the maximum deviation value of DC voltage and the maximum deviation value of AC power grid, respectively.

The virtual inertia time constant of MMC-HVDC H_{MMC} can be obtained as:

$$H_{\mathrm{MMC}} = \frac{k_{\mathrm{c}}}{2} C_{\mathrm{eq}} U_{\mathrm{dc0}} \tag{5}$$

The H_{MMC} serves as a critical metric for quantifying the inertial capacity of the MMC-HVDC system to resist frequency fluctuations under power imbalance conditions. A larger value of this constant indicates a greater abundance of storable energy and available inertial resources within the system, contributing to more effective maintenance of system frequency stability.

3.2 Virtual Inertia Control Based on WT Rotor Kinetic Energy

In the MMC-HVDC system, the energy supply capacity of the storage elements is constrained by the DC voltage stability margin. To enhance the system's inertia support capability and further mitigate the frequency change rate, a VIC strategy and its parameter design method are proposed for differentiated utilization of WT frequency regulation capacity. By introducing indicators related to the DC terminal voltage of the sending-end MMC into the active power control loop of WTs, a correlation expression between the angular velocity and the DC voltage is constructed. This not only realizes the differentiated utilization of rotor kinetic energy but also enhances the inertia support level of the system.

Under normal operating conditions, the output power of the DFIG is:

$$P_{wind} = k_{opt}\omega_d^3 \tag{6}$$

where k_{opt} is the maximum power tracking coefficient; ω_d is the current rotational speed.

When the system frequency drops, the DC voltage will decrease accordingly. Each DFIG increases its output active power by reducing the rotor speed, which is equivalent to adding a virtual capacitor ΔC_{vir} on the DC side of the MMC-HVDC, thereby improving the inertia level. This process is shown in Eqs. (7)–(9). Since the change in the WT rotor speed is small, $\Delta\omega^2$ and $\Delta\omega^3$ can be ignored.

$$\begin{aligned}\Delta P &= k_{opt}\omega_d^3 - k_{opt}\omega_{d0}^3 \\ &= k_{opt}\left(3\omega_{d0}^2\Delta\omega - 3\omega_{d0}\Delta\omega^2 + \Delta\omega^3\right) \\ &\approx 3k_{opt}\omega_{d0}^2\Delta\omega\end{aligned} \tag{7}$$

$$\Delta P \approx 3k_{opt}\omega_{d0}^2\Delta\omega = \Delta C_{vir}U_{dc}\frac{dU_{dc}}{dt} \tag{8}$$

$$\Delta\omega = U_{dc}\frac{\Delta C_{vir}U_{dc}}{3k_{opt}\omega_{d0}^2}\frac{dU_{dc}}{dt} = k_d\frac{dU_{dc}}{dt} \tag{9}$$

where ΔP is the additional active power generated during the WT's power support phase; ω_{d0} is the initial rotational speed; $\Delta\omega = \omega_d - \omega_{d0}$ is the change in rotational speed of the WT before and after participating in inertia support; k_d is the coupling coefficient between $\Delta\omega$ and dU_{dc}/dt.

The operational flow of the VIC strategy is illustrated in Fig. 2: When the system is subjected to disturbances, frequency fluctuations occur in the receiving-end power grid. Leveraging the coupled relationship between DC voltage and power grid frequency established in Eq. (3), the power grid frequency fluctuation information is transmitted to the wind farm side in real time using DC voltage as the transmission medium. Subsequently, as shown in Eq. (9), the DC voltage change rate dU_{dc}/dt on the wind farm side MMC (WFMMC) side is introduced into the active power control loop of each DFIG in the wind farm, enabling the DFIGs to actively adjust their active power output, respond rapidly to the sudden frequency change of the receiving-end power grid, and provide inertia support for the system.

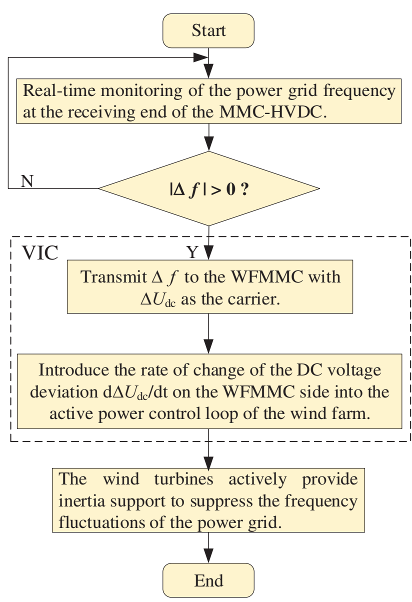

Figure 2: Implementation flow chart of the VIC strategy

According to the above analysis, after considering the inertia support of DFIGs, Eq. (1) can be further modified to Eq. (10). It can be observed that when DFIGs and the MMC-HVDC system are treated as an integrated unit, the participation of DFIGs in energy regulation is equivalent to increasing the equivalent capacitance of MMC-HVDC, thereby jointly suppressing system frequency fluctuations, so as to increase the equivalent inertia time constant H_{eq}, as shown in Eq. (11). Compared with existing single-resource inertia support control, it can effectively suppress frequency abrupt change to improve system frequency stability.

$$\left(C_{eq} + \Delta C_{vir}\right) U_{dc} \frac{dU_{dc}}{dt} = P_{in} - P_{out} \tag{10}$$

$$H_{eq} = \frac{k_c}{2} \left(C_{eq} + \Delta C_{vir}\right) U_{dc0} \tag{11}$$

4 Coordinated Recovery Strategy for MMC-HVDC Connecting Offshore Wind Farms Considering Secondary Frequency Drop

During the inertia support phase, to maintain the DC voltage of MMC-HVDC constant, the electromagnetic power output by the WTs increases, resulting in a power imbalance on both sides of the turbine, which leads to a decrease in rotational speed. Once the preset rotational speed recovery condition is met, the WT will automatically exit the inertia support control. At this point, its output power drops sharply, the DC voltage value decreases, and the risk of a secondary frequency drop in the system increases. Therefore, based on the energy margin of the capacitor in the MMC-HVDC, a coordinated speed recovery method for system of MMC-HVDC connecting offshore wind power is proposed. Through the coordinated control of the two, the above-mentioned instantaneous power drop is alleviated, thereby avoiding secondary frequency drops and shortening the rotor speed recovery time of WTs.

4.1 Adaptive Speed Recovery Strategy Based on Variable Droop Coefficient

From the swing equation, when P_m and P_e reach equilibrium, it can be inferred that the rotational speed change rate will turn positive in the subsequent moment, that is, the rotational speed converges. To prevent the WTs from stalling and tripping off the grid due to prolonged inertia support for the system, this paper designates the moment of rotor speed convergence as the timing for WTs to exit frequency regulation, with the criterion shown in Eq. (12).

$$\left|\omega\left(t + T\right) - \omega\left(t\right)\right| \leq 4 \times 10^{-7} \tag{12}$$

where T is the sampling period of the WT rotor speed; $\omega(t)$ is the current rotational speed (the notation "t" is added to distinguish the current moment from the next moment).

In this paper, a comprehensive inertia control strategy is adopted for WTs. During the inertia support phase, proportional and differential links are introduced to provide additional power ΔP_{add}:

$$\Delta P_{add} = k_d \frac{dU_{dc}}{dt} + k_p \Delta U_{dc} \tag{13}$$

where k_d and k_p are the coupling coefficients between the additional power and the DC voltage-related indicators, respectively; both can be designed based on the current rotational speed of WTs and the safety limits of the corresponding variables. It can be seen from this that ΔP_{add} is closely related to the control parameters k_p and k_d. Considering that after the frequency (DC voltage) crosses the lowest point, the power adjustment generated by the differential link is positive and will gradually decrease to 0 as the frequency recovers, this process is beneficial to the recovery of the WT rotor speed. Therefore, here only the adjustment of the proportional coefficient k_p is considered to slow down the power drop rate of the WT during the recovery period.

Considering the differences in rotor kinetic energy released by WTs under different wind speed scenarios, to achieve rapid and stable rotational speed recovery, the droop coefficient is adjusted following the "first slow then fast" principle during the recovery phase to slow down the rate of power drop. Specifically, the DC voltage deviation ΔU_{dc} (i.e., Δf) is used as an intermediate variable to reflect the system operating state, and the logistic function is multiplied by a fixed droop coefficient. This avoids secondary frequency drops while increasing the rotor speed recovery rate. The specific expression is as follows:

$$k_p' = k_p\left(\frac{K_{max}K_0 e^{nt}}{K_{max} + K_0\left(e^{nt} - 1\right)}\right) = k_p K\left(t\right) \tag{14}$$

$$t = \frac{\Delta U_{dc} - \Delta U_{dcmin}}{\Delta U_{dcmax} - \Delta U_{dcmin}} \tag{15}$$

where k_p is the proportional coefficient after the WT exits the inertia support control; $K(t)$ is a time-varying function; K_{max} is set to 1; K_0 is set to 0.0001; n is set to 27; ΔU_{dcmax} and ΔU_{dcmin} are the limit values of DC voltage deviation.

It can be known from Eq. (13) that when the WT operates again on the MPPT curve, the WT switches to the maximum power point tracking mode, and its rotational speed can naturally recover to the initial operating state. The specific control method is shown in Fig. 3.

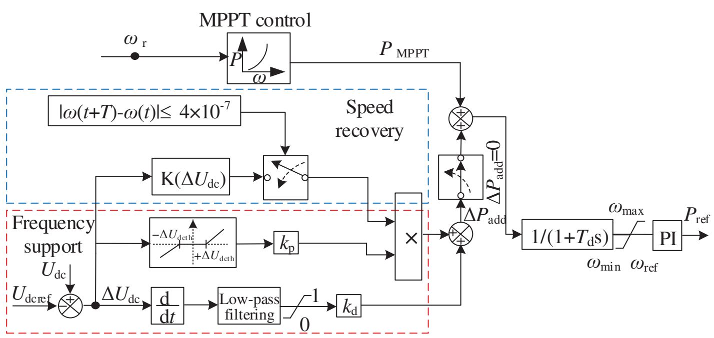

Figure 3: Frequency response model of systems containing energy storage

In summary, after reaching the preset speed recovery condition, the power impact on the receiving-end power grid can be fundamentally reduced by adjusting the control parameters of WTs. It can be known from Eqs. (14) and (15) that in this process, ΔU_{dc} directly affects the output power of WTs and the speed recovery. The recovery speed of WTs rotational speed can be further improved by exploiting the voltage support capability of the MMC capacitor.

4.2 Strategy for Suppressing Secondary Frequency Drops Based on SM Adaptive Switching

The energy storage of the MMC-HVDC mainly relies on the electric field energy in the capacitors, and its energy is positively correlated with the SM capacitance and the capacitor voltage. In engineering practice, a voltage safety margin is generally reserved in the selection of SM capacitors. The IEC 61071 standard stipulates that under non-locking conditions, the upper limit of the short-term withstand voltage of a SM capacitor is set to 1.5 times the rated voltage. At this time, the available stored energy for inertia support can reach 2.25 times the rated capacity. This setting not only ensures the safety of SM capacitors and various power devices but also provides reliable energy support at critical moments. Meanwhile, in practical applications, the number of SMs in the sending and receiving end converter stations usually has a margin of 0.08, and the response time for realizing SM switching is relatively short, enabling rapid power support.

In the current control mode of the MMC-HVDC, since the total number of inserted SMs in the upper and lower arms is constant (N remains unchanged), SM capacitor voltages vary synchronously with the DC voltage, confining their fluctuation range entirely within the DC-voltage safety margin and severely constraining the full utilization of the system's inherent regulation potential.

To more rapidly and effectively mitigate the abrupt power change during WT rotor speed recovery, and to minimize the resulting power impact on the system, this paper separately designs adaptive SM switching strategies for the rectifier- and inverter-side MMCs of the MMC-HVDC system, as shown by the blue dashed line in Fig. 1. The moment condition (12) is satisfied, the rectifier-side MMC adjusts the number of inserted SMs according to the WT rotor speed recovery state and its released rotor kinetic energy. This not only collaborates with the turbine to reduce the power drop magnitude but also supplies energy support for the turbine to reach its optimal operating speed. When DC-voltage fluctuations are small, DC current accurately reflects power changes; therefore, the inverter-side MMC adaptively adjusts the number of inserted SMs based on DC-current variation once a preset condition is met, achieving coordination without communication. In addition, a high-pass filter is introduced so that SM counts in both converter-side and inverter-side MMCs return to their initial values after the system stabilizes. The expression for the number of inserted SMs in the rectifier-side MMC is:

$$N_{\mathrm{WFMMC}} = \mathrm{round}\left(N_0 + 0.08 \times \left(\frac{\omega_{\mathrm{d}}^2 - \omega_{\min}^2}{\omega_{\mathrm{d0}}^2 - \omega_{\min}^2}\right) N_0\right) \tag{16}$$

where N_0 is the initial number of inserted SMs in the rectifier-side MMC; $\omega_{\min}$ is the WT's minimum speed limit; 0.08 is the per-unit redundancy of SM count in practical MMC; round(x) denotes the rounding function.

To realize communication-free activation of the receiving-end MMC control, the activation conditions for SM switching of the receiving-end MMC are designed based on the variation characteristics of DC voltage and current, with the expressions as follows:

$$\begin{cases} \dfrac{\mathrm{d}U_{\mathrm{dc}}}{\mathrm{d}t} > \lambda_1 \\ \dfrac{\mathrm{d}I_{\mathrm{dc}}}{\mathrm{d}t} < \lambda_2 \end{cases} \tag{17}$$

where λ_1 and λ_2 are the activation thresholds.

The number of inserted SMs in the inverter-side MMC is:

$$N_{\mathrm{GSMMC}} = \mathrm{round}\left(N_0 \times (1 - k\Delta I_{\mathrm{dc}})\right) \tag{18}$$

where ΔI_{dc} is the variation of DC current; k is the proportional coefficient, whose value is designed according to the maximum deviation of the number of SMs in the receiving-end MMC $\Delta N_{\mathrm{GSMMCmax}}$ and the maximum deviation of DC current $\Delta I_{\mathrm{dcmax}}$, as shown in Eq. (19):

$$k = \frac{\Delta N_{\mathrm{GSMMCmax}}}{\Delta I_{\mathrm{dcmax}}} \tag{19}$$

It can be seen that, during WT rotor speed recovery, adjusting the number of inserted SMs in both rectifier- and inverter-side MMC not only achieves coordinated control between the source and the grid, but also effectively prevents secondary frequency drops while accelerating speed restoration.

5 Simulation Verification

A model of the MMC-HVDC-connected offshore wind power grid integration system is established in Matlab/Simulink, as shown in Fig. 1, and simulations are performed on the real-time digital simulation platform RTLAB OP5707XG-8. The sending end is an offshore wind farm with a total installed capacity of 600 MW (comprising two 300 MW DFIGs), and the receiving end is an 1800 MW synchronous generation system (comprising two 900 MW synchronous generators). The key system parameters are listed in Table 1. The effectiveness of the above-mentioned control method is analyzed below under the load step-in operating condition.

When the system is in a steady state, the two WTs operate at wind speeds of 9.5 m/s, and the coordination thresholds ΔU_{dcth} is set to 0.003, the total active power output of the wind farm reaches 697 MW, and the loads 1 and 2 of the receiving-end AC grid are 710 and 100 MW, respectively. When t = 50 s, Load2 is connected, resulting in a significant drop in the grid frequency. To comprehensively evaluate the effect of the coordinated recovery method, three scenarios are set as follows: Scenario 1: The WT recovers its speed naturally; Scenario 2: Only the speed recovery strategy is adopted for the WT; Scenario 3: The control method proposed in [14] is adopted; Scenario 4: MMC-HVDC and wind power cooperate to support speed recovery. The simulation results are shown in the following figures.

5.1 Simulation Analysis of Case 1

To verify the effectiveness of the coordinated recovery method proposed in this paper, a simulation analysis is conducted under Case 1 (with Load2 set to 100 MW), and the simulation results are shown in Fig. 4.

It can be seen that after Load2 is connected, the frequency of the receiving-end power grid drops rapidly. Since Scenarios 2, 3 and 4 switch to the relevant control at the moment when the WT meets the speed recovery condition (with t_{off} = 59 s), the response characteristics of each scenario are the same in the first 59 s. In Scenario 1, as no control is adopted, the phenomenon of secondary frequency drop is serious, with the magnitude of the secondary frequency reduction reaching approximately 0.0008 p.u. However, in Scenarios 2, 3 and 4, the output power of the WT changes slowly at 59 s, which does not cause obvious power impact on the system, and the frequency can smoothly reach the steady-state level, as shown in Fig. 4a; In addition, a comparison between Scenario 3 and Scenario 4 shows that Scenario 3 employs fewer SMs, which leads to increased DC voltage fluctuations and, consequently, a larger fluctuation amplitude of the receiving-end frequency. However, in Scenario 4, by adopting a "slow-then-fast" speed regulation of the WT droop coefficient and the MMC-HVDC recovery strategy illustrated in Fig. 4b, the SM capacitor voltage is reduced by 0.073 p.u., and the number of SMs in operation is increased to 246, representing an 8.77% increment. This enables full utilization of its redundancy, thereby rapidly compensating for the transient power deficit, as shown in Fig. 4c–e. Thus, the full recovery time of the WT output power and rotor speed is shortened by 4 s compared with that in Scenario 2, as shown in Fig. 4f,g. The results demonstrate that by adjusting the wind-power drop rate and the number of SMs in the rectifier- and inverter-side MMC, capacitor energy and rotor kinetic energy can be fully exploited to shorten turbine speed-recovery time and effectively suppress secondary frequency dips.

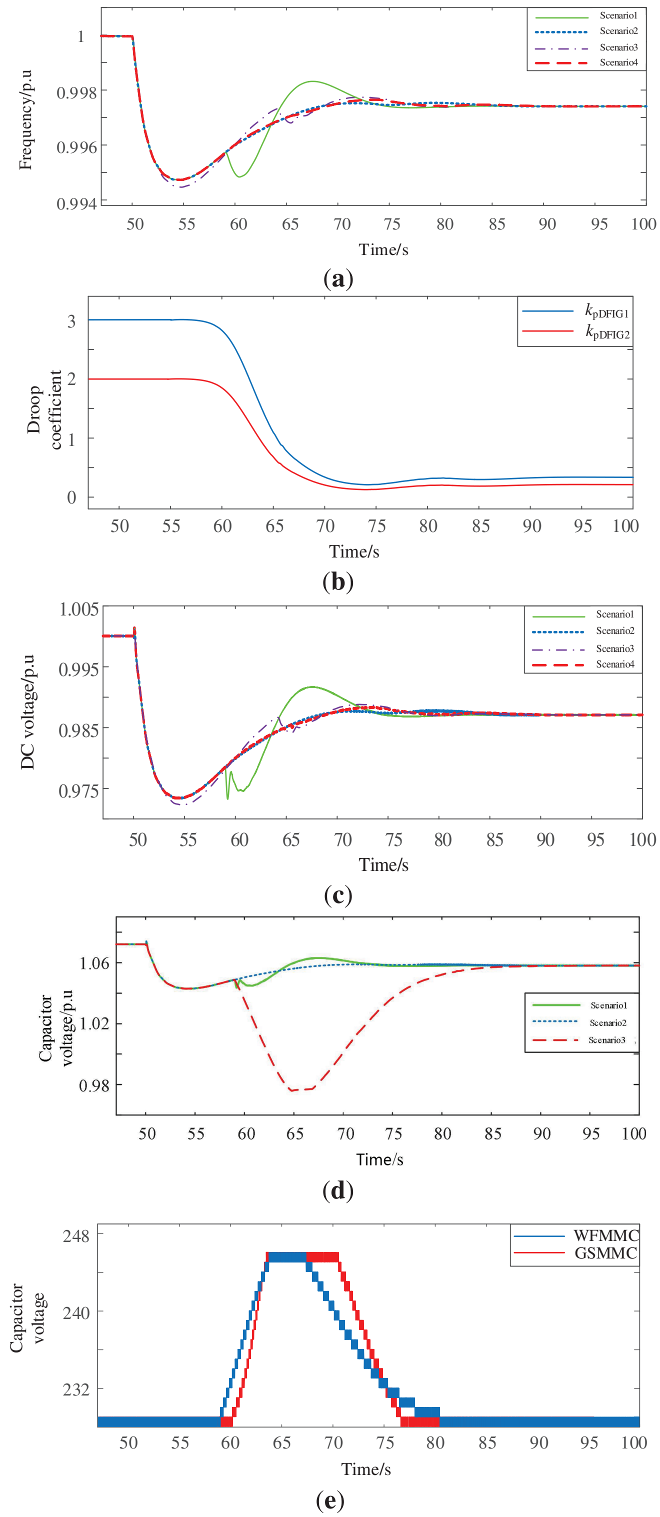

Figure 4: (Continued)

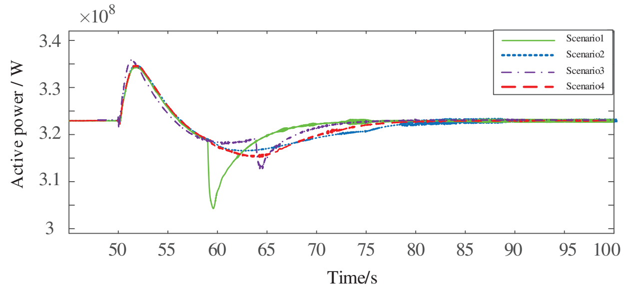

(**f**)

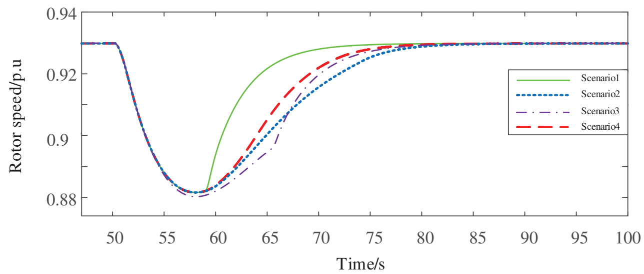

(**g**)

Figure 4: Simulation results of case 1. (**a**) Frequency of the receiving-end grid; (**b**) coefficient of frequency control; (**c**) DC voltage; (**d**) capacitor voltage; (**e**) number of bridge arm SMs; (**f**) output power of WT generator 2; (**g**) rotor speed of WT generator 2

5.2 Simulation Analysis of Case 2

To verify the effectiveness of the coordinated recovery method proposed in this paper under different scenarios, a simulation analysis is performed under Case 2 (with Load2 set to 150 MW, the wind speed increased to 10 m/s, and the active power at the sending end balanced). The simulation results are shown in Fig. 5.

According to the simulation results, after increasing the system load, the frequency drops severely, the magnitude of the secondary frequency drop is approximately 0.0013 p.u., representing a 62.5% increase compared with that in case 1. Among them, the system characteristics under Scenarios 1, 3 and 4 are the same as those mentioned above, and will not be repeated here. However, in Scenario 2, since the WT control parameters adopt a fixed-coefficient recovery, the output power of the WT still decreases relatively rapidly at the moment of switching control. Similar to Scenario 1, Scenario 2 inevitably experiences a secondary frequency drop, as shown in Fig. 5a. Meanwhile, Fig. 5b reveals the relationship between system power imbalance and frequency changes. In Scenarios 1 and 2, the instantaneous drop in the WT's output power is large, reaching 20 and 8 MW, respectively, which simultaneously causes a secondary drop in frequency. Another difference from Case 1 is that in Case 2, the time for the WT's rotational speed to recover to its initial value is prolonged by 5 s, and a smooth recovery cannot be achieved, as shown in Fig. 5c. It can thus be concluded that when the system disturbance is large, the method adopted in Scenario 2 is no longer applicable. However, under the proposed recovery control method, no secondary frequency dip occurs, which is mainly attributed to the rapid support provided by the capacitor energy. The specific principle is explained as follows: the number of inserted SMs increases correspondingly, and the average voltage of the capacitor in a single SM decreases synchronously. This not only reserves a larger regulation margin for the system but also enhances the regulation capability of the flexible HVDC system, reducing the power impact on the power grid.

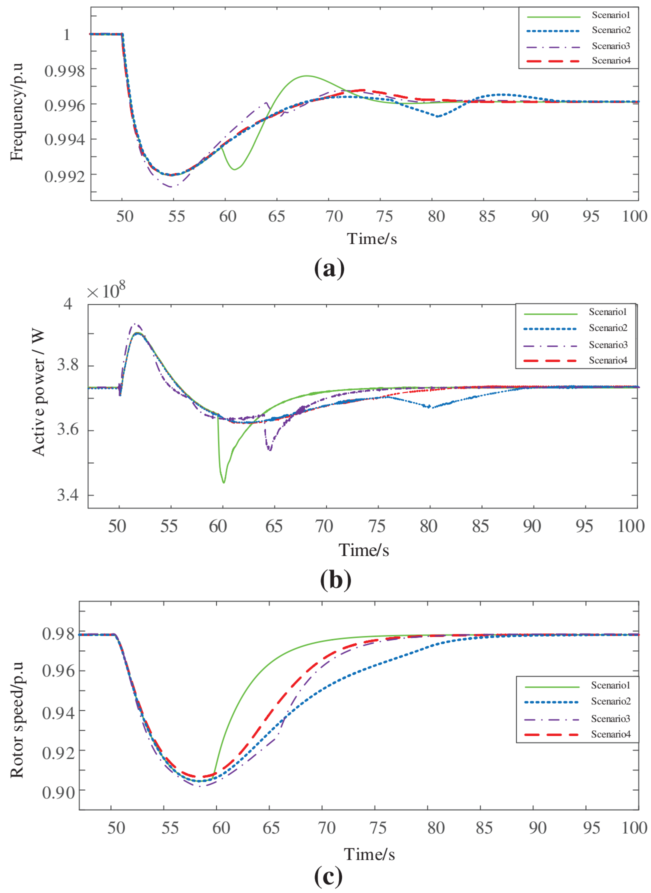

Figure 5: Simulation results of case 2. (**a**) Frequency of the receiving-end grid; (**b**) output power of WT generator 2; (**c**) rotor speed of WT generator 2

6 Conclusion

Focusing on the frequency safety challenges in the power-electronic-dominated power system, this paper proposes a coordinated control strategy and corresponding parameter tuning methods to improve the system inertia level and avoid secondary frequency drops, which enhances the recovery speed of WT rotor speed while maintaining the safe and stable operation of the system frequency. Through simulation analysis, the following conclusions are drawn:

(1) In terms of inertia support, by establishing the connection among frequency, rotational speed, and DC voltage, the coordinated support of system inertia by DC capacitors and WT rotors is realized. This not only effectively suppresses the frequency change rate at the initial stage of disturbance but also achieves the differentiated utilization of the WT's frequency modulation capability.

(2) In terms of WT rotor speed recovery, by enhancing the control dimensions of the sending-end and receiving-end MMCs, the operating range of the SM capacitor voltage is adjusted. Cooperating with the adaptive adjustment of the WT's proportional coefficient, this not only effectively avoids the secondary frequency drop but also shortens the recovery time of the WT's rotor speed.

Acknowledgement: The authors thank the Northeast Electric Power University for conducting this research.

Funding Statement: This research was supported by State Grid Corporation of China (grant number SGNXJY00ZWJS2500029).

Author Contributions: The authors confirm contribution to the paper as follows: Yi Qi: Funding acquisition, study design. Yuhao Xie: Validation, original draft. Zhibing Hu: Project administration. Fan Ding: Data analysis. Junxian Ma: Supervision. Liang Zhao: Software. Shouqi Jiang: Methodology. All authors reviewed the results and approved the final version of the manuscript.

Availability of Data and Materials: Data will be made available on request.

Ethics Approval: Not applicable.

Conflicts of Interest: The authors declare no conflicts of interest to report regarding the present study.

References

1. Raza MW, Raza M, Badia JG, Prieto-Araujo E, Gomis-Bellmunt O. Fault handling capabilities of grid-forming wind turbines in offshore wind farms connected with MMC HVDC system. IEEE Access. 2024;12:36404–14. doi:10.1109/ACCESS.2024.3373478.
2. Yu Z, Song Q, Yuan Z, Zou C, Qiao X, Liu W. Transmission topology and control for ultra-large offshore wind bases integrating multiple offshore low-frequency AC links and onshore HVDC link. IEEE Trans Power Deliv. 2024;39(5):2797–809. doi:10.1109/TPWRD.2024.3432897.
3. Li L, Li Q, Jiang Y, Zhang Y, Xie Y, Wang Z. Small-signal stability analysis of offshore wind farm integrated grid-forming VSC-HVDC system. In: Proceedings of the 2023 IEEE 7th Conference on Energy Internet and Energy System Integration (EI2); 2023 Dec 15–18; Hangzhou, China. p. 57–62. doi:10.1109/EI259745.2023.10513037.
4. Ji K, Tang G, Pang H, Yang J. Impedance modeling and analysis of MMC-HVDC for offshore wind farm integration. IEEE Trans Power Deliv. 2020;35(3):1488–501. doi:10.1109/tpwrd.2019.2946450.
5. Liu Y, Lin Z, Xu C, Wang L. Fault ride-through hybrid controller for MMC-HVDC transmission system via switching control units based on Bang-Bang funnel controller. J Mod Power Syst Clean Energy. 2023;11(2):599–610. doi:10.35833/mpce.2021.000470.
6. Li Y, Zhu M, Chao P, Li W, Sun B. An improved frequency modulation method for fault ride through of MMC-HVDC systems connected DFIG wind farms. In: Proceedings of the 2018 2nd IEEE Conference on Energy Internet and Energy System Integration (EI2); 2018 Oct 20–22; Beijing, China. p. 1–6. doi:10.1109/EI2.2018.8582295.
7. Wang X, Yang R, Shi Z, Cai X, Shi X, Chen Y. Coordinated low voltage ride-through of MMC-HVDC transmission system and wind farm with distributed braking resistors. IEEE Access. 2022;10:87860–9. doi:10.1109/ACCESS.2022.3200370.
8. Lin H, Xue T, Lyu J, Cai X. Impact of different AC voltage control modes of wind-farm-side MMC on stability of MMC-HVDC with offshore wind farms. J Mod Power Syst Clean Energy. 2023;11(4):1687–99. doi:10.35833/mpce.2022.000363.
9. Li Y, Lu Y, Yang J, Yuan X, Yang R, Yang S, et al. Transient stability of power synchronization loop based grid forming converter. IEEE Trans Energy Convers. 2023;38(4):2843–59. doi:10.1109/tec.2023.3283396.
10. Xue T, Lyu J, Wang H, Cai X. A complete impedance model of a PMSG-based wind energy conversion system and its effect on the stability analysis of MMC-HVDC connected offshore wind farms. IEEE Trans Energy Convers. 2021;36(4):3449–61. doi:10.1109/TEC.2021.3074798.
11. Sun K, Xiao H, Liu S, Liu Y. Machine learning-based fast frequency response control for a VSC-HVDC system. CSEE J Power Energy Syst. 2020;7(4):688–97. doi:10.17775/cseejpes.2020.01410.
12. Lu GL, Lin CH, Wu YK. Comparison of communication-based and coordination-based frequency control schemes for HVdc-connected offshore wind farms. IEEE Trans Ind Appl. 2021;57(4):3352–65. doi:10.1109/tia.2021.3079233.
13. Liu X, Lindemann A. Control of VSC-HVDC connected offshore windfarms for providing synthetic inertia. IEEE J Emerg Sel Top Power Electron. 2018;6(3):1407–17. doi:10.1109/jestpe.2017.2751541.
14. Jiang S, Wang H, Li G, Xin Y, Wang L, Xu Y. A novel coordinated control strategy for frequency regulation of MMC-HVDC connecting offshore wind farms. IEEE Trans Sustain Energy. 2024;15(2):1028–38. doi:10.1109/tste.2023.3323813.

15. Ma Z, Wang X, Wu S, Zhang X. Coordinated control strategy of offshore wind farm and MMC-HVDC to improve the inertia level of power system. In: Proceedings of the 2019 IEEE 8th International Conference on Advanced Power System Automation and Protection (APAP); 2019 Oct 21–24; Xi'an, China. p. 1819–23. doi:10.1109/apap47170.2019.9224753.
16. Chu J, Lv Y, Xu Y, Du G, Sun D, Yu P. Coordinated control strategy for improving frequency stability of offshore wind farms connected to the grid through MMC-HVDC transmission. In: Proceedings of the 2022 4th Asia Energy and Electrical Engineering Symposium (AEEES); 2022 Mar 25–28; Chengdu, China. p. 354–60. doi:10.1109/AEEES54426.2022.9759790.
17. Wen Y, Zhan J, Chung CY, Li W. Frequency stability enhancement of integrated AC/VSC-MTDC systems with massive infeed of offshore wind generation. IEEE Trans Power Syst. 2018;33(5):5135–46. doi:10.1109/TPWRS.2018.2792906.
18. Jose K, Adeuyi O, Liang J, Ugalde-Loo CE. Coordination of fast frequency support from multi-terminal HVDC grids. In: Proceedings of the 2018 IEEE International Energy Conference (ENERGYCON); 2018 Jun 3–7; Limassol, Cyprus. p. 1–6. doi:10.1109/ENERGYCON.2018.8398852.
19. Adeuyi OD, Cheah-Mane M, Liang J, Jenkins N. Fast frequency response from offshore multiterminal VSC-HVDC schemes. IEEE Trans Power Deliv. 2017;32(6):2442–52. doi:10.1109/tpwrd.2016.2632860.
20. Qu L, Qiao W. Constant power control of DFIG wind turbines with supercapacitor energy storage. IEEE Trans Ind Appl. 2011;47(1):359–67. doi:10.1109/tia.2010.2090932.
21. Huang Z, Wu W, Lin C, Guo Z. Cooperative strategies for frequency control of wind turbines to mitigate secondary frequency dip: coefficient allocation and exit techniques. IEEE Trans Sustain Energy. 2025;16(2):1056–67. doi:10.1109/TSTE.2024.3498006.
22. Chen W, Zheng T, Nian H, Yang D, Yang W, Geng H. Multi-objective adaptive inertia and droop control method of wind turbine generators. IEEE Trans Ind Appl. 2023;59(6):7789–99. doi:10.1109/tia.2023.3307368.
23. Wu Z, Gao DW, Zhang H, Yan S, Wang X. Coordinated control strategy of battery energy storage system and PMSG-WTG to enhance system frequency regulation capability. IEEE Trans Sustain Energy. 2017;8(3):1330–43. doi:10.1109/TSTE.2017.2679716.
24. Zhou Z, Li H, Tan H. Coordinated frequency control strategy of offshore wind farm via MMC-HVDC considering secondary frequency drop. In: Proceedings of the 2023 26th International Conference on Electrical Machines and Systems (ICEMS); 2023 Nov 5–8; Zhuhai, China. p. 1977–80. doi:10.1109/ICEMS59686.2023.10344365.
25. Lu Z, Ye Y, Qiao Y. An adaptive frequency regulation method with grid-friendly restoration for VSC-HVDC integrated offshore wind farms. IEEE Trans Power Syst. 2019;34(5):3582–93. doi:10.1109/TPWRS.2019.2901986.